

GEOMETRIC INFLIGHT CALIBRATION OF THE STEREOSCOPIC CCD-LINESCANNER MOMS-2P

Wolfgang Kornus, Manfred Lehner, Manfred Schroeder

German Aerospace Center (DLR)
Institute of Optoelectronics, Optical Remote Sensing Division
D-82230 Wessling, Germany
e-mail: Wolfgang.Kornus@dlr.de, Manfred.Lehner@dlr.de, ms@zeus.oe.dlr.de
Commission I, Working Group 3

ABSTRACT

This paper describes the geometric inflight calibration of the Modular Optoelectronic Multispectral Scanner MOMS-2P, which is collecting digital multispectral and threefold along track stereoscopic imagery of the earth's surface from the PRIRODA module of the Russian space station MIR since October 1996. Goal is the verification and, if necessary, the update of the calibration data, which were deduced from the geometric laboratory calibration. The paper is subdivided into two parts, describing two different procedures of geometric inflight calibration: The first method is based on DLR matching software and is restricted to nadir looking channels, which are read out simultaneously. From very many individual point matches between the images of the same area taken by the different CCD arrays the most reliable ones are specially subselected and used to calculate shifts with components in and across flight direction between the CCD arrays. These actual shifts are compared to the nominal shifts, derived from the results of the laboratory calibration, and parameters of the valid camera model are estimated from both data sets by least squares adjustment. A special case of band to band registration are the two optically combined CCD-arrays of the high resolution channels. They are read out simultaneously with a nominal 10 pixel overlap in stereoscopic imaging mode A. The DLR matching software is applied to calculate the displacement vector between the two CCD-arrays. The second method is based on combined photogrammetric bundle adjustment using an adapted functional model for the reconstruction of the interior orientation. It requires precise and reliable ground control information as well as navigation data of the navigation-package MOMSNAV. 11 subsequent image scenes of MOMS-2P data take T083C are evaluated, which were taken in March 1997 building an about 550 km long strip over southern Germany and Austria. From both procedures calibration data are deduced, which are presented and compared to the lab-calibration results.

1 INTRODUCTION

MOMS-2P is a pushbroom scanner for multispectral and along-track stereoscopic imaging in four different modes. It is built by the German Daimler-Benz Aerospace Company Dasa and mounted on the Priroda module of the Russian space station Mir since May 1996. It delivers imagery since end of September 1996 (no imagery since May 1997 because of problems with camera and Mir station). MOMS-2P is the refurbished MOMS-02 camera which has been flown on space shuttle during D2 mission in April/May 1993.

The optical system of MOMS is based on a modular concept. The multispectral module comprises two nadir oriented lenses, containing two CCD-arrays each for colour image acquisition in four narrow banded spectral channels with 18 m ground pixel size. The stereo module consists of 3 lenses, which are oriented in three different directions. The forward and aft looking lens contain one CCD array each for panchromatic image acquisition with 18 m ground pixel size. The third lens is nadir looking and contains two CCD-arrays, which are optically combined to one high resolution channel, providing panchromatic imagery with a ground pixel size of 6 m. The complexity and also the high weight (143 kg) of the optical module posed high demands on the process of laboratory calibration, which was conducted by Dasa. Experience from D2 mission showed that for this big camera with five different lenses inflight geometric calibration activities are necessary. In this paper two different methods of inflight calibration are described: The first method is restricted to channels which are simultaneously read out while nominally looking nadir. These are channels 1, 2, 3, 4, and 5A (or subarrays hereof) in certain combinations in the imaging

modes B, C, and D (see [2]). Here, DLR matching software has been used to calculate displacement vectors with components in and across flight direction (rows, columns). These measurements are produced with subpixel accuracy by local least squares matching techniques using a special evaluation strategy for the matching results to cope with the (generally wanted!) dissimilarities between the images of the diverse multispectral channels. The second method is based on photogrammetric bundle adjustment and therefore is restricted to channels of the stereo imaging modes (A and D). In this example channels 5A, 5B, 6 and 7 of imaging mode A are involved. The approach can be considered as the reverse process of photogrammetric point determination using precise navigation data and also a substantial amount of very accurate ground control information in order to estimate the camera geometry. From both methods parameters of the valid camera model are estimated from the inflight and laboratory measurements by least squares adjustment. From the derived camera parameters new calibration tables are deduced as input for the Level 1A*- and Level 1B processing at DLR Neustrelitz and for photogrammetric evaluation of stereoscopic MOMS-2P imagery

2 INFLIGHT CALIBRATION OF CHANNELS 1, 2, 3, 4 and 5A

The image based band to band registration method used here has already been applied to MOMS-02 on D2 mission (1993). For MOMS-2P it has been refined to provide a full displacement function over the applicable range of image pixels (columns) of the CCD sensor arrays which is different for the individual imaging modes. Because natural displacements

may occur between different bands of a sensor for objects with distinctively different reflection in the respective wavelength intervals a strategy has to be found to exclude such object areas from this evaluation. Of course, all images used have been radiometrically corrected (L1A products). Measurement tools and evaluation strategy are explained in the following subsections.

2.1 Image matching

The DLR matching software has been developed for the automated measurement of massive numbers of conjugate points in the stereoscopic imagery of 3-line stereo scanners (projects MEOSS and MOMS). More details about this software can be found in [10], [11], and [5].

The main features used here are:

1. an interest operator selects well defined patterns suitable for digital image correlation; the principles of the Förstner interest operator are used with slight modification; a good interest operator point is defined by a surrounding window with multidirectional edge information and a local contrast above a given threshold
2. conjugate points on pixel accuracy level are generated using the maximum of the normalized correlation coefficient; the latter and a quality figure describing the steepness and uniqueness of the peak in the matrix of correlation coefficients are stored for later subselection of conjugate points; the positioning of the search areas is done via an affine transformation which is calculated using already known conjugate points in the neighbourhood (normally, an image pyramid is used for getting these approximate points)
3. local least squares matching (LLSQM) is finally used for refinement of the conjugate points to subpixel accuracy; in this step it is also possible to match images of different resolution like MOMS high and low resolution channels

2.2 Evaluation strategy

The steps for the extraction of the shifts between the MOMS-2P channels are:

1. **interest operator points** are generated for one channel; the interest operator will avoid areas with low contrast and patterns with ambiguous matching results; typical pattern size used is 7 x 7 pixel
2. run the **matching software** for the channel combination under investigation: a search area size of 19 x 19 pixel is used for the matching at pixel accuracy; for search area selection it is sufficient to use an estimated mean shift between the channels which was determined beforehand and is valid for all data takes; local least squares matching is run twice using **two** different window sizes (15 x 15 and 17 x 17 pixels have been used) for subpixel registration
3. consider both resulting point files selecting only points which satisfy the following conditions:
 - (a) maximum of correlation coefficient and quality figure (from areal correlation with pixel accuracy; see [9]) are beyond given thresholds (0.9

and 0.23, respectively, have been used throughout this evaluation to guarantee well defined objects)

- (b) local least squares matching converged for both window sizes (take well defined objects only)
 - (c) differences between the resulting coordinates for the two window sizes are below a given threshold (exclusion of objects with different patterns in the different spectral bands; 0.25 pixel has been used throughout the investigation)
4. **averaging:** the image matching results in irregularly distributed sets of conjugate point pairs (l, c) for one channel and (l', c') for the other channel. The differences $l-l'$ (along-track) and $c-c'$ (across-track) define the local shifts between the channels. In order to even more reduce the impact of natural channel differences these shifts are averaged for a number of equidistant column intervals (one column imaged by one CCD-array element) of about 200 pixel. The mean values and their standard deviations are then assigned to the centers of the column intervals.

Thus, displacement functions have been derived for all channel pairs for a number of data takes. These functions enter an adjustment process combining laboratory calibration and matching results to give final valid calibration tables and camera parameters (see chapter 2.6).

2.3 Example

Figure 1 shows the image of channel 3 (red) of scene 3 (part of Ethiopia) of data take T081A imaged on December 18, 1996 in imaging mode B (4 multispectral channels, 5800 pixel per channel, 5920 image lines per scene). This is a good scene for the measurements discussed in this paper. The interest operator found about 173,000 points (centers of pattern areas) in the image of channel 3 (see Figure 2), about 83 percent of which could be located in the other channels by the image matching software.



Figure 2: Interest operator points in a 300x400 pixel subscene of T081A, scene 3, channel 3

The mean values of the maximum of the correlation coefficients and the quality figure are shown in Table 1. Table 2

and different bands of a scene for objects with
low contrast in the scene. The objects are
detected by using a threshold on the difference
image.

- (a) low level thresholding is performed for each
window size (the well defined objects only)
- (b) difference between the resulting coordinates for
the two window sizes are below a given threshold

objects in different bands of a scene for objects with
low contrast in the scene. The objects are
detected by using a threshold on the difference
image. Of course, it might be useful to
use a different threshold for different bands.
This is the idea of the proposed method. More
details are given in the following sections.

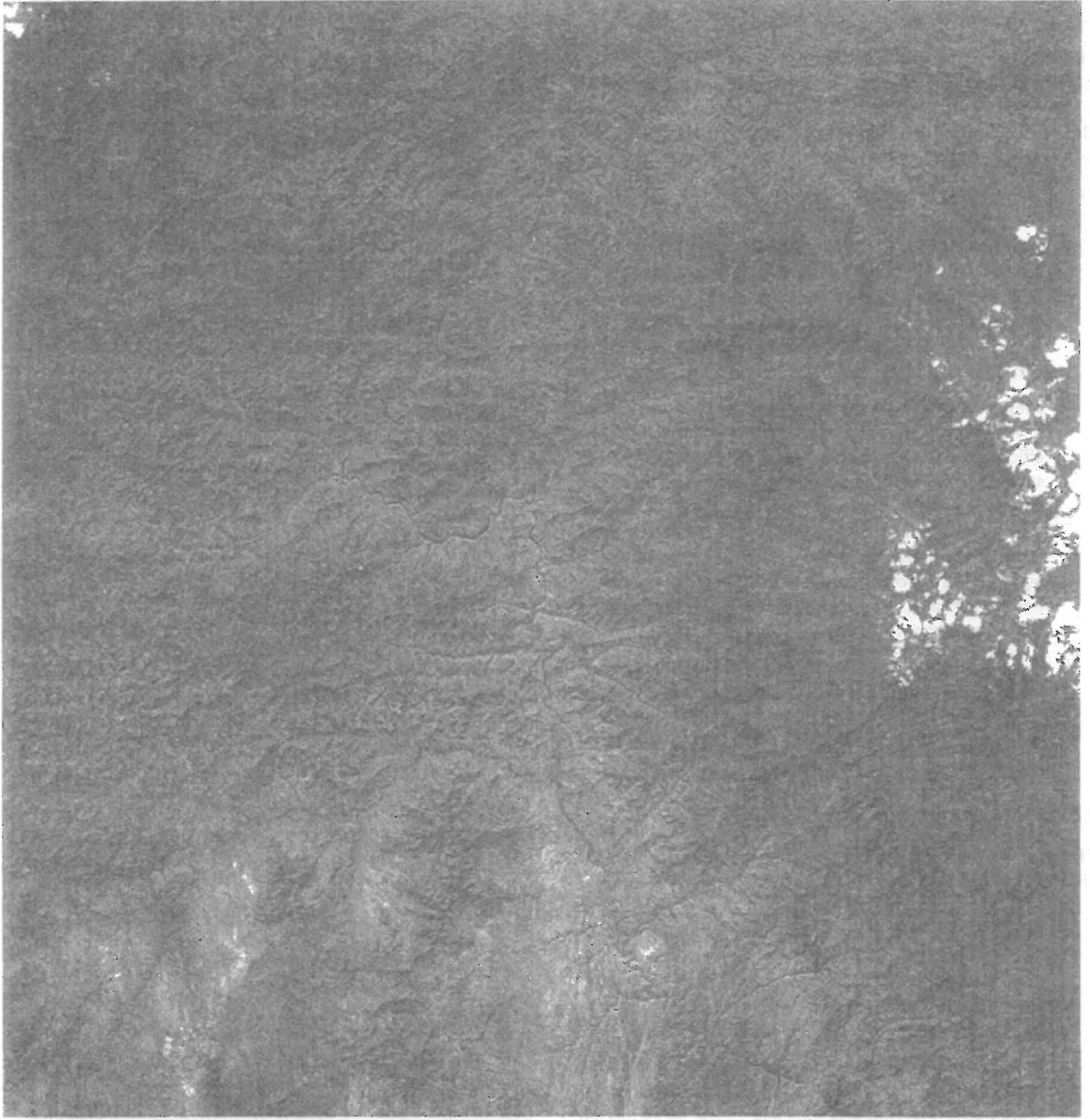


Figure 1: MOMS-2P Ethiopia: data take T081A, scene 3, channel 3, about 104km x 106km

| channel pair | ch3/ch1 | ch3/ch2 | ch3/ch4 |
|---------------------|---------|---------|---------|
| mean correl. coeff. | 0.92 | 0.93 | 0.89 |
| mean quality figure | 0.28 | 0.27 | 0.25 |

Table 1: T081A, scene 3, mean correlation coefficient and quality figures

shows the shifts between channels 2 and 3 as the results of the evaluation for 29 column intervals. The graphical representation is given in Figure 3. More results for different channel

| interval number | nr. of points | center column | mean shift | | stand.dev. | |
|-----------------|---------------|---------------|------------|------|------------|------------|
| | | | x | y | σ_x | σ_y |
| 1 | 2939 | 100.98 | 1.40 | 6.31 | 0.14 | 0.16 |
| 2 | 3126 | 300.95 | 1.42 | 6.31 | 0.12 | 0.16 |
| 3 | 3195 | 500.91 | 1.46 | 6.37 | 0.11 | 0.16 |
| 4 | 3369 | 700.88 | 1.49 | 6.48 | 0.10 | 0.13 |
| 5 | 3659 | 900.84 | 1.51 | 6.59 | 0.11 | 0.14 |
| 6 | 3579 | 1100.81 | 1.53 | 6.71 | 0.11 | 0.14 |
| 7 | 3328 | 1300.78 | 1.55 | 6.84 | 0.11 | 0.12 |
| 8 | 3426 | 1500.74 | 1.60 | 6.98 | 0.10 | 0.13 |
| 9 | 3419 | 1700.71 | 1.63 | 7.13 | 0.10 | 0.14 |
| 10 | 3504 | 1900.67 | 1.66 | 7.29 | 0.13 | 0.15 |
| 11 | 3573 | 2100.64 | 1.68 | 7.41 | 0.12 | 0.15 |
| 12 | 3495 | 2300.60 | 1.71 | 7.54 | 0.11 | 0.14 |
| 13 | 3944 | 2500.57 | 1.75 | 7.65 | 0.12 | 0.13 |
| 14 | 4257 | 2700.53 | 1.79 | 7.74 | 0.12 | 0.13 |
| 15 | 4648 | 2900.50 | 1.85 | 7.80 | 0.12 | 0.14 |
| 16 | 5174 | 3100.47 | 1.94 | 7.88 | 0.12 | 0.13 |
| 17 | 5031 | 3300.43 | 2.06 | 7.97 | 0.12 | 0.13 |
| 18 | 5580 | 3500.40 | 2.21 | 8.07 | 0.11 | 0.12 |
| 19 | 5368 | 3700.36 | 2.32 | 8.16 | 0.11 | 0.13 |
| 20 | 3842 | 3900.33 | 2.42 | 8.24 | 0.11 | 0.14 |
| 21 | 3115 | 4100.29 | 2.56 | 8.31 | 0.11 | 0.14 |
| 22 | 3490 | 4300.26 | 2.70 | 8.39 | 0.10 | 0.12 |
| 23 | 4048 | 4500.22 | 2.82 | 8.47 | 0.10 | 0.12 |
| 24 | 4155 | 4700.19 | 2.97 | 8.54 | 0.12 | 0.12 |
| 25 | 4550 | 4900.16 | 3.16 | 8.61 | 0.12 | 0.10 |
| 26 | 3835 | 5100.12 | 3.33 | 8.65 | 0.13 | 0.10 |
| 27 | 3720 | 5300.09 | 3.51 | 8.72 | 0.12 | 0.11 |
| 28 | 4780 | 5500.05 | 3.68 | 8.77 | 0.12 | 0.11 |
| 29 | 4519 | 5700.02 | 3.85 | 8.80 | 0.12 | 0.11 |

Table 2: T081A, scene 3: shifts channel 2 - channel 3; the points for each column interval stem from an image subarea of about 200 x 5920 pixel; x is along track (rows), y is along scan line (columns)

combinations, data takes and imaging modes are given in [12].

2.4 Particularities of the different imaging modes

For an exact definition of the imaging modes of the MOMS-2P camera see [1].

- Mode A:** the panchromatic channels 5, 6, and 7 do all look in different directions in one instant of time, thus, the method mentioned above is not applicable; there is only a very small overlap of the high resolution chan-

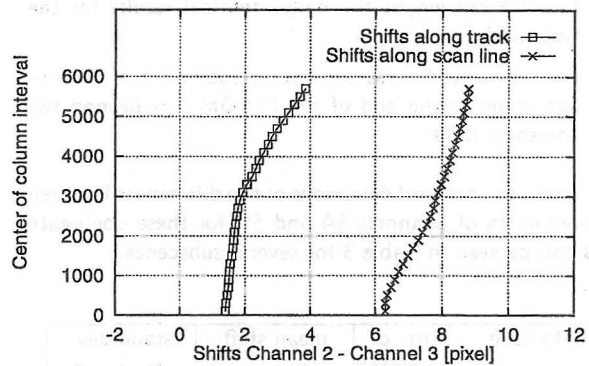


Figure 3: T081A, scene 3: shifts between channels 2 and 3

nel 5A and 5B of nominally 10 pixels which can help in the composition of a really continuous channel 5 array (there is an obvious shift between the two channels of about 1 pixel along and 2 pixel across flight direction). The values of important camera parameters for these stereo channels can only be estimated by photogrammetric adjustment in the presence of very good knowledge of the terrain and precise orbit and attitude data (see chapter 3).

- Mode B:** the pairwise shifts between the multispectral channels 1, 2, 3, and 4 over the full length of the 5800 active pixels can be measured
- Mode C:** the pairwise shifts between the multispectral channels 2, 3, and 4 over 3220 active pixels can be measured; the shifts to channel 5A can be measured for a subarray of 2000 pixels of these 3220 pixels; the latter measurement is done in two steps: a first matching is carried out between the multispectral channels and a corresponding reduced resolution image of the high resolution channel (factor 3 reduction in both directions); this results in initial approximations for a multi-scale matching between channel 5A and the multispectral channels
- Mode D:** the shifts between the multispectral channels 1 and 4 can be measured over the full length of the 5800 active pixels; the stereo channels 6 and 7 are not simultaneously looking onto the same terrain (up to now no data take is available in this mode which could be evaluated for inflight geometric calibration with photogrammetric methods).

2.5 Registration between channels 5A and 5B

Channels 5A and 5B are optically coupled to form the high resolution channel 5. These two channels are read out with a nominal overlap of 10 pixel. Via image matching shifts in and across flight direction of 1.2 and -1.9 pixel were measured (see [13]). For these measurements the overlap area was 8 times enlarged by bilinear interpolation to get meaningful window sizes for LLSQM. The latter was performed for a regular set of initial approximations. Two window sizes, 37x37 and 41x41 pixel, have been used. Only those conjugate points entered into the calculation of shifts for which the following two conditions applied;

1. LLSQM converged to nearly identical results for the two window sizes
2. the normalized cross correlation coefficient of the image chips at the end of the LLSQM was beyond the threshold 0.89

The means and standard deviations of the differences between the coordinates of channels 5A and 5B for these conjugate points can be seen in Table 3 for several subscenes.

| data take | nr. of points | mean shift | | stand.dev. | |
|--------------|---------------|------------|-------|------------|------------|
| | | x | y | σ_x | σ_y |
| T0700/part 1 | 115 | 1.18 | -1.89 | 0.26 | 0.26 |
| T0700/part 2 | 135 | 1.12 | -1.90 | 0.24 | 0.29 |
| T07FB/part 1 | 57 | 1.16 | -1.79 | 0.19 | 0.19 |
| T07FB/part 2 | 58 | 1.20 | -1.79 | 0.21 | 0.23 |
| all | 365 | 1.16 | -1.86 | 0.23 | 0.26 |

Table 3: result of matching in overlap area of channels 5A and 5B (imaging mode A); part 1/2 are upper and lower half of the scenes; this separation was made for visualizing the accuracy potential of the matching; x is along track (rows), y is along scan line (columns)

2.6 Generation of calibration tables

The matching results differ from the values of the laboratory calibration (see [6]) to an extent (partly several pixels) that makes it necessary to change the calibration tables for the systematic processing of the MOMS images. As an example Figure 4 shows a comparison of the shifts between channels 2 and 3 derived from laboratory calibration versus the results of image matching. Here, the differences of about 1.8 pixel in the along track shifts e.g. indicate that the along track components of the camera parameters in channel 2 and/or channel 3 have changed to that extent since time of lab-calibration. The different angles between the y-axis and the curves representing the along scan line shifts indicate changes in the image scale, which correspond to changes in the focal lengths of channel 2 and/or channel 3.

If the relative shifts are determined for a variety of possible channel combinations, camera parameters for all investigated channels can be derived with respect to the parameters of a selected reference channel (see Table 4). For that purpose, the differences x_{diff} and y_{diff} between the shifts derived from lab-calibration and from image matching were fed into a least squares adjustment, estimating parameters of an adjusting line in case of the along scan line shifts or an adjusting parabola in case of the along track shifts. The correction equations read:

$$v_x = x_{diff} - [d\hat{A}_x + d\hat{B}_x y]$$

$$v_y = y_{diff} - [d\hat{A}_y + d\hat{B}_y y + d\hat{C}_y y^2]$$

with y denoting the y-coordinate (along scan line) of the respective center of column interval with respect to the center of the CCD-array.

This was done for 20 different channel combinations in imaging modes B and C (see [7]) involving the four multispectral channels and also the high resolution channel 5A. Then, the

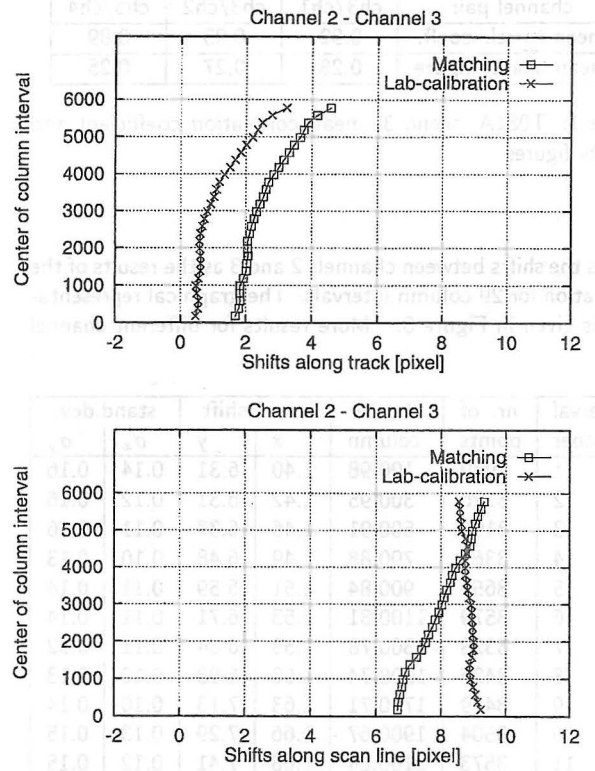


Figure 4: Shifts between channels 2 and 3: matching versus laboratory calibration results

parameters $d\hat{A}_x$, $d\hat{B}_x$, $d\hat{A}_y$, $d\hat{B}_y$, and $d\hat{C}_y$ were transformed into the 5 parameters dx_0 , dy_0 , $d\kappa$, dc and dK , describing deviations of camera parameter differences between the two selected channels, which obviously occurred since time of lab-calibration. The notification is in accordance to the lab-calibration evaluation (see [6]), where a set of 5 camera parameters has been considered for each channel:

- the deviation of the focal length c ,
- the coordinates of the principal point x_0 and y_0 ,
- the sensor curvature K and
- the sensor rotation within the image plane κ .

The mentioned deviations for the respective channel combination is obtained as follows:

$$dc = c d\hat{B}_x$$

$$dx_0 = d\hat{A}_x$$

$$dy_0 = d\hat{A}_y$$

$$dK = d\hat{C}_y$$

$$d\kappa = \frac{1}{1+\hat{B}_y^2} d\hat{B}_y \approx d\hat{B}_y$$

The 20 investigated channel combinations resulted in 20 camera parameter differences, which correspond to camera parameter changes of altogether 5 channels. By least squares adjustment a final set of camera parameters for each channel was estimated from these differences, while the lab-calibrated parameters of one selected channel were taken as reference. Due to the small swath of imaging mode C, the sensor curvature K only was determined for the 4 multispectral channels

in imaging mode B. Table 4 contains the estimated camera parameters \hat{x} and the theoretical standard deviations $\hat{\sigma}_x$ resulting from the adjustment of the camera parameter differences. The column Δx reflects the deviations from the lab-calibrated results. Boldfaced characters indicate reference values taken from lab-calibration.

| MS1 | | \hat{x} | $\hat{\sigma}_x$ | Δx |
|----------|---------|----------------|------------------|--------------|
| c | [mm] | 220.139 | 0.003 | -0.021 |
| x_0 | [pixel] | 7.4 | 0.078 | 2.4 |
| y_0 | [pixel] | -1.3 | 0.057 | -0.6 |
| K | [pixel] | 0.3 | 0.012 | -0.1 |
| κ | [mdeg] | 2.1 | 1.783 | -3.5 |
| MS2 | | \hat{x} | $\hat{\sigma}_x$ | Δx |
| c | [mm] | 220.076 | 0.003 | -0.019 |
| x_0 | [pixel] | 7.2 | 0.048 | 0.2 |
| y_0 | [pixel] | -1.0 | 0.044 | -1.4 |
| K | [pixel] | -0.6 | 0.014 | 0.3 |
| κ | [mdeg] | 2.7 | 1.763 | -6.5 |
| MS3 | | \hat{x} | $\hat{\sigma}_x$ | Δx |
| c | [mm] | 219.964 | 0.002 | -0.151 |
| x_0 | [pixel] | 15.1 | 0.027 | -0.8 |
| y_0 | [pixel] | 1.3 | 0.048 | 0.0 |
| K | [pixel] | 0.2 | — | 0.0 |
| κ | [mdeg] | -21.9 | 1.763 | -7.6 |
| MS4 | | \hat{x} | $\hat{\sigma}_x$ | Δx |
| c | [mm] | 219.951 | 0.003 | -0.140 |
| x_0 | [pixel] | 14.5 | 0.056 | -0.8 |
| y_0 | [pixel] | 0.7 | 0.052 | 1.3 |
| K | [pixel] | 0.5 | 0.016 | 0.0 |
| κ | [mdeg] | -22.8 | 1.796 | -6.1 |
| HR5 | | \hat{x} | $\hat{\sigma}_x$ | Δx |
| c | [mm] | 660.256 | — | 0.000 |
| x_0 | [pixel] | -0.4 | — | 0.0 |
| y_0 | [pixel] | 0.1 | — | 0.0 |
| K | [pixel] | -0.3 | — | — |
| κ | [mdeg] | -2.9 | — | 0.0 |

Table 4: Results of adjustment; Reference parameters are marked by boldfaced characters

K represents the along track effect caused by sensor curvature at $y = 3000$ pixel, i.e. at the edges of the 6000 pixel long CCD-arrays. The along track effect caused by a sensor rotation of $\kappa = 10$ mdeg is about 0.5 pixel at $y = 3000$ pixel. For comparison, the camera parameters deduced from the lab-calibration evaluation (see [6], [8]) are listed in Table 5:

| | MS1 | MS2 | MS3 | MS4 | HR5A |
|-----------------|---------|---------|---------|---------|---------|
| c [mm] | 220.160 | 220.095 | 220.115 | 220.091 | 660.256 |
| x_0 [pixel] | 5.0 | 7.0 | 15.9 | 15.3 | -0.4 |
| y_0 [pixel] | -0.7 | 0.4 | 1.3 | -0.6 | 0.1 |
| K [pixel] | 0.417 | -0.936 | 0.199 | 0.481 | -0.312 |
| κ [mdeg] | 5.654 | 9.207 | -14.306 | -16.738 | -2.915 |

Table 5: Lab-calibrated camera parameters

3 INFLIGHT CALIBRATION OF CHANNELS 5A, 5B, 6 and 7

Originally this task was planned to be conducted in cooperation with the Spanish Institut Cartogràfic de Catalunya (ICC) using MOMS-2P imagery of Catalonia. From the ICC database, containing a country-wide digital terrain model and also digital orthoimages in scale 1: 25000, a large number of ground control points should have been derived in an automated way (see [5]). Since a suitable data take of Catalonia has not been registered so far, the imagery of southern Germany and Austria, taken in April 1997, is processed instead.

3.1 Input data

The image data set comprises 11 radiometrically corrected level-1A scenes #25 to #35. The total length of the strip is about 550 km corresponding to 30568 image lines. 3800 equally distributed tie points were derived by local least squares image matching in all three image strips.

As ground control information navigation points of the AMil-Geo (Amt fuer militaerisches Geowesen) were used, representing street crossings or junctions, which normally can well be identified also in medium resolution satellite imagery. Their object coordinates are known with an accuracy of 1.5 m in X, Y and Z. At the Chair for Photogrammetry and Remote Sensing of the Technical University Munich 181 navigation points were manually measured in the nadir looking channel. Figure 5 shows the distribution of both the tie points and the ground control points. Up to now the availability of control points is restricted to the German part of the image strip (until image scene #30).

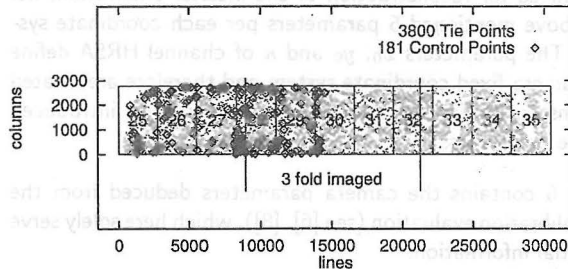


Figure 5: Distribution of tie and control points in image scenes #25 to #35

The identification accuracy was adversely affected by defocussing effects, which occurred in the high resolution channel. They probably were caused by thermal instabilities of the sensor due to an insufficient warming up time prior to the data take. Nevertheless it was preferred to conduct the measurements in the defocussed high resolution imagery rather than in the 3 times decreased resolution of the oblique viewing stereo channels. After identification the image points were automatically transferred to the other image strips by a multi-scale matching approach (see [5]). For the future it is also planned to check these measurements stereoscopically using both oblique viewing channels

The data of the navigation package MOMSNAV were pre-processed at the German Space Operation Center (GSOC) of DLR and at the GeoForschungsZentrum (GFZ) Potsdam. GSOC provided a set of 3 Euler angles for each image frame with a relative accuracy of about $10''$. At GFZ Potsdam

orbit determination using the GPS raw data of MOMSNAV resulted in a time series (1 Hz) of orbit positions with an absolute accuracy of about 5 m and a relative accuracy of about 3 m [4]. All navigation data were provided with reference to the corotating, earth-centered WGS-84 coordinate system

3.2 Bundle adjustment

The functional model of the bundle adjustment is based on extended collinearity equations, which have been adapted to the specific MOMS line imaging geometry. A detailed description of the model extensions is given in [3]. The exterior orientation parameters are estimated only for so-called orientation images, which are introduced at constant time intervals. Between the orientation images the temporal course of the exterior orientation parameters is modeled by a third order polynomial. Navigation data are introduced as uncorrelated observations of the exterior orientation parameters. Systematic errors in these data like biases and linear drifts are treated as additional unknowns, which are estimated simultaneously with the other unknowns in the adjustment.

The model of the interior orientation is characterized by different image coordinate systems, which can be assigned to different lenses or even different channels of MOMS-2P. In this example four coordinate systems are involved, which are assigned to the two oblique viewing stereo channels ST6 and ST7 and the two nadir viewing high resolution channels HR5A and HR5B. The two HR-channels are treated separately, since the analysis of the HR-imagery indicated a slight relative movement between the HR5A- and HR5B-CCD-arrays (see chapter 2.5). Altogether 20 parameters are introduced for reconstruction of the interior orientation; i.e. the above mentioned 5 parameters per each coordinate system. The parameters x_0 , y_0 and κ of channel HR5A define the camera-fixed coordinate system and therefore are treated as constants. The remaining 17 parameters are introduced as free unknowns.

Table 6 contains the camera parameters deduced from the lab-calibration evaluation (see [6], [8]), which here solely serve as initial information:

| | HR5A | HR5B | ST6 | ST7 |
|-----------------|---------|---------|---------|---------|
| c [mm] | 660.256 | 660.224 | 237.241 | 237.246 |
| x_0 [pixel] | 0.1 | 0.2 | -7.2 | -0.5 |
| y_0 [pixel] | -0.4 | 0.1 | 8.0 | 19.2 |
| K [pixel] | -0.3 | -0.4 | -1.1 | 1.7 |
| κ [mdeg] | -2.9 | 5.4 | -1.5 | -1.4 |

Table 6: Lab-calibrated camera parameters

Table 7 gives an overview of all observations and their a priori standard deviations which were introduced into the bundle adjustment. The observations of the exterior orientation parameters were interpolated for the times of the orientation images. An interval of 4600 image lines, corresponding to 11.3 seconds flight time, led to 8 orientation images, which proved to be sufficient to model the temporal course of these parameters.

| observations | | type | a priori σ |
|--------------|-----------------|--------------------|-------------------|
| 3800 | tie points | image coordinates | 0.3 Pixel |
| 181 | control points | image coordinates | 0.3 Pixel |
| 181 | control points | object coordinates | 1.5 m |
| 8x3 | attitude angles | ext. orientation | 10'' |
| 8x3 | positions | ext. orientation | 3 m |
| 3 | position biases | ext. orientation | 5 m |

Table 7: Observations introduced into the bundle adjustment

3.3 Results

Table 8 contains the estimated camera parameters \hat{x} and the theoretical standard deviations $\hat{\sigma}_x$ as result of the bundle adjustment. The column Δx reflects the deviations from the lab-calibrated results in Table 6. Significant deviations are marked by boldfaced characters.

| HR5A | | \hat{x} | $\hat{\sigma}_x$ | Δx |
|----------|---------|----------------|------------------|---------------|
| c | [mm] | 660.201 | 0.022 | -0.055 |
| x_0 | [pixel] | 0.1 | — | 0.0 |
| y_0 | [pixel] | -0.4 | — | 0.0 |
| K | [pixel] | 0.2 | 0.3 | 0.5 |
| κ | [mdeg] | -2.9 | — | 0.0 |
| HR5B | | \hat{x} | $\hat{\sigma}_x$ | Δx |
| c | [mm] | 660.217 | 0.021 | -0.007 |
| x_0 | [pixel] | 0.2 | 0.2 | 0.0 |
| y_0 | [pixel] | -0.1 | 0.1 | -0.2 |
| K | [pixel] | 1.3 | 0.3 | 1.7 |
| κ | [mdeg] | 12.6 | 11.4 | 7.2 |
| ST6 | | \hat{x} | $\hat{\sigma}_x$ | Δx |
| c | [mm] | 237.176 | 0.006 | -0.065 |
| x_0 | [pixel] | -5.1 | 0.2 | 2.1 |
| y_0 | [pixel] | 6.1 | 1.2 | -1.9 |
| K | [pixel] | 1.7 | 0.5 | 2.8 |
| κ | [mdeg] | -12.4 | 7.3 | -10.9 |
| ST7 | | \hat{x} | $\hat{\sigma}_x$ | Δx |
| c | [mm] | 237.234 | 0.005 | -0.012 |
| x_0 | [pixel] | 1.1 | 0.2 | 1.6 |
| y_0 | [pixel] | 21.3 | 1.2 | 2.1 |
| K | [pixel] | -0.5 | 0.4 | -2.2 |
| κ | [mdeg] | -13.2 | 7.7 | -11.8 |

Table 8: Results of bundle adjustment; Significant deviations from lab-calibration are marked by boldfaced characters

The results demonstrate, that changes of the camera geometry obviously did occur since the time of lab-calibration. This is not too astonishing, since the analysis of the multispectral images also showed deviations from the lab-calibration results of up to 2.4 pixel (see chapter 2).

Regarding the theoretical standard deviations, the camera parameters are determined with rather high accuracy. The standard deviations of the parameters y_0 and κ will further improve if the number of ground control points is increased. That was found by computer simulations, which were conducted in preparation of this investigation (see [5]). Table 8 still must be regarded as preliminary. Final results will be presented after further extension of the ground control point network and also after verification of the point identification by stereoscopic measurements.

4 CONCLUSIONS

It has been demonstrated that inflight calibration activities are necessary for the MOMS-2P camera. It is shown that sufficiently accurate measurements for band to band registration can be carried out using image matching techniques. First results using stereoscopic mode A imagery demonstrated that inflight calibration by photogrammetric bundle adjustment is also possible. The evaluation however suffers from the uncertainties of control point identification as a consequence of the defocussed high resolution imagery. In order to achieve more reliable results, the ground control point network still needs to be extended and also verified by stereoscopic measurements using imagery of the oblique viewing stereo channels.

It was planned to repeat the inflight geometric calibration regularly throughout the mission. This need for a constant surveillance is also emphasized by deviations of the measurements of the along-track shifts between the channels of the two multispectral lenses for first experimental data takes and later ones (not reported here, see [12]).

5 ACKNOWLEDGMENTS

We wish to thank AMilGeo for kindly making available the control data and also Timm Ohlhof and Elmar Putz from the Chair for Photogrammetry and Remote Sensing, TU Munich for organizing and conducting the control point measurements. The work presented in this paper is funded by grant 50EE9529 of the German Space Agency (DARA).

REFERENCES

- [1] Dasa Company Document Nr. M2P-DAS-200-RS-001: "MOMS-2P: Re-design performance and system requirements specification", Dasa 1.2.1996
- [2] "MOMS-2P: Data User Handbook", German Aerospace Center (DLR), German Remote Sensing Data Center (DFD), January 1997
- [3] H. Ebner, W. Kornus, T. Ohlhof: "A simulation study on point determination for the MOMS-02/D2 space project using an extended functional model", *Geo-Informationssysteme*, February 1994, pp. 11-16.
- [4] S. Föckersperger., R. Hollmann., G. Dick, C. Reigber: "On Board MIR: Orienting Remote Images with MOMS-NAV", *GPS World*, October 1997.
- [5] W. Kornus, M. Lehner, F. Blechinger, E. Putz: "Geometric Calibration of the Stereoscopic CCD-Linescanner MOMS-2P", *Int. Archives of Photogrammetry and Remote Sensing, Vol. 31, Part B1*, pp. 90-98, Vienna, Austria, 1996.
- [6] W. Kornus: "MOMS-2P Geometric Calibration Report - Results of laboratory calibration (Version 1.1)", DLR, Institute of Optoelectronics, December 1996.
- [7] W. Kornus: "MOMS-2P: Geometric Calibration - Results of band to band registration (Version 1.2)", DLR, Institute of Optoelectronics, December 1996
- [8] W. Kornus: "MOMS-2P Geometric Calibration Report - Results of channel 5A/5B registration (Version 1.3)", DLR, Institute of Optoelectronics, May 1997.
- [9] M. Lehner: "Triple stereoscopic imagery simulation and digital image correlation for MEOSS project", *International Archives of Photogrammetry and Remote Sensing, Vol. 27, Part 1*, pp. 477-484, Stuttgart, 1986

- [10] M. Lehner, R.S. Gill: "Semi-Automatic Derivation of Digital Elevation Models from Stereoscopic 3-Line Scanner Data", *International Archives of Photogrammetry and Remote Sensing, Vol.29, Part B4*, pp. 68-75, Washington, 1992
- [11] M. Lehner, W. Kornus: "The photogrammetric evaluation of MOMS-02/D2 mode 3 data (Mexico, Ethiopia)", *Proceedings of SPIE Conference on Remote Sensing and Reconstruction for 3-D Objects and Scenes*, pp. 102-114, San Diego, USA, 9./10. 7. 1995.
- [12] M. Lehner: "MOMS-2P inflight geometric calibration - measurements for band to band registration based on digital image matching", DLR, Institute of Optoelectronics, December 1996
- [13] M. Lehner: "MOMS-2P inflight geometric calibration - measurements for registration of channels 5A/5B based on digital image matching", DLR, Institute of Optoelectronics, February 1997
- [14] P. Seige, P. Reinartz, M. Schroeder: "The MOMS-2P mission on the MIR station", *International Archives of Photogrammetry and Remote Sensing, Vol. 32, Part 1*, Bangalore, India, 23.-27. 2. 1998.